Regular high-frequency pulsation modes in young intermediate-mass stars

Timothy R. Bedding[1,2], Simon J. Murphy[1,2], Daniel R. Hey[1,2], Daniel Huber[3], Tanda Li[1,2,4], Barry Smalley[5], Dennis Stello[6,2], Timothy R. White[1,2,7], Warrick H. Ball[4,2], William J. Chaplin[4,2], Isabel L. Colman[1,2], Jim Fuller[8], Eric Gaidos[9], Daniel R. Harbeck[10], J. J. Hermes[11], Daniel L. Holdsworth[12], Gang Li[1,2], Yaguang Li[1,2,13], Andrew W. Mann[14], Daniel R. Reese[15], Sanjay Sekaran[16], Jie Yu[17], Victoria Antoci[2], Christoph Bergmann[6], Timothy M. Brown[10], Andrew W. Howard[8], Michael J. Ireland[7], Howard Isaacson[18], Jon M. Jenkins[19], Hans Kjeldsen[2], Curtis McCully[10], Markus Rabus[10,20], Adam D. Rains[7], George R. Ricker[21], Christopher G. Tinney[6] & Roland K. Vanderspek[21]

[1]*Sydney Institute for Astronomy (SIfA), School of Physics, University of Sydney, 2006, Australia*
[2]*Stellar Astrophysics Centre, Department of Physics and Astronomy, Aarhus University, 8000 Aarhus C, Denmark*
[3]*Institute for Astronomy, University of Hawai'i, 2680 Woodlawn Drive, Honolulu, HI 96822, USA*
[4]*School of Physics and Astronomy, University of Birmingham, Birmingham B15 2TT, UK*
[5]*Astrophysics Group, Lennard-Jones Laboratories, Keele University, Staffordshire ST5 5BG, United Kingdom*
[6]*School of Physics, University of New South Wales, 2052, Australia*
[7]*Research School of Astronomy and Astrophysics, Mount Stromlo Observatory, The Australian National University, Canberra, ACT 2611, Australia*
[8]*TAPIR, Mailcode 350-17, California Institute of Technology, Pasadena, CA 91125, USA*
[9]*Department of Earth Sciences, University of Hawai'i, Honolulu HI 96822, USA*
[10]*Las Cumbres Observatory Global Telescope, 6740 Cortona Dr., Suite 102, Goleta, CA 93111, USA*
[11]*Department of Astronomy, Boston University, 725 Commonwealth Ave., Boston, MA 02215, USA*
[12]*Jeremiah Horrocks Institute, University of Central Lancashire, Preston PR1 2HE, UK*
[13]*Department of Astronomy, Beijing Normal University, Beijng 100875, China*
[14]*Department of Physics and Astronomy, University of North Carolina at Chapel Hill, Chapel Hill, NC 27599-3255, USA*
[15]*LESIA, Observatoire de Paris, PSL Research University, CNRS, Sorbonne Universités, UPMC Univ. Paris 06, Univ. Paris Diderot, Sorbonne Paris Cité, 5 place Jules Janssen, 92195 Meudon, France*
[16]*Instituut voor Sterrenkunde (IvS), KU Leuven, Celestijnenlaan 200D, 3001 Leuven, Belgium*
[17]*Max-Planck-Institut für Sonnensystemforschung, Justus-von-Liebig-Weg 3, 37077 Göttingen, Germany*
[18]*Department of Astronomy, University of California at Berkeley, Berkeley, CA 94720-3411, USA*
[19]*NASA Ames Research Center, Moffett Field, CA, 94035, USA*
[20]*Department of Physics, University of California, Santa Barbara, CA 93106-9530, USA*
[21]*Department of Physics, and Kavli Institute for Astrophysics and Space Research, Massachusetts Institute of Technology, Cambridge, MA 02139, USA*

Accepted for publication in *Nature*

Asteroseismology is a powerful tool for probing the internal structures of stars by using their natural pulsation frequencies[1]. It relies on identifying sequences of pulsation modes that can be compared with theoretical models, which has been done with great success for many classes of pulsators including low-mass solar-type stars[2], red giants[3], high-mass stars[4] and white dwarfs[5]. However, a large group of pulsating stars of intermediate mass—the so-called δ Scuti stars—have rich pulsation spectra for which systematic mode identification has not been possible[6,7]. This arises because only a seemingly random subset of possible modes are excited, and because rapid rotation tends to spoil the regular patterns[8–10]. Here we report the detection of remarkably regular sequences of high-frequency pulsation modes in 60 intermediate-mass main-sequence stars, allowing definitive mode identification and opening up a new regime in which the power of asteroseismology can be applied to determine masses, ages and internal structure. Some of these stars have space motions that indicate they are members of known associations of young stars, and modelling of their pulsation spectra confirms that these stars are indeed young.

The δ Scuti variables are stars of intermediate mass (1.5–2.5 $M_\odot$) that pulsate in low-order pressure modes[6,7]. Observations have shown that many δ Scuti stars have regular frequency spacings in their pulsation spectra (references given in Methods) but a large sample with unambiguous mode identifications is lacking. Each pulsation mode in a non-rotating star is identified by two integers: the radial order, n, and the degree, l. We expect the strongest observable modes to be of low degree ($l = 0$, 1 and 2), since higher degrees have greatly reduced amplitudes due to cancellation in disk-integrated light. In the so-called asymptotic regime ($n \gg l$), modes with a given degree l are approximately equally spaced in frequency by a separation, $\Delta\nu$, that is the inverse of the time taken for sound waves to travel through the star and is approximately proportional to the square root of the mean stellar density[1].

The patterns are more complex in a rotating star, with the mode frequencies also depending on the azimuthal order, m. Each nonradial ($l \geq 1$) mode in the pulsation spectrum is split into $2l + 1$ components, where m ranges from $-l$ to l. The relative amplitudes of these components depend on the inclination of the rotation axis to the line of sight. For example, if a star is seen at low inclination (close to pole-on) then the axisymmetric ($m = 0$) mode in each multiplet will dominate, leading to a simpler pulsation spectrum. In very rapidly rotating stars, the oblateness alters the pulsation cavity and further complicates the pattern. However, for rotation rates less than $\sim$50% of Keplerian break-up, the radial modes ($l = 0$) and the axisymmetric dipolar modes ($l = 1$, $m = 0$) are still expected to follow a regular spacing that is similar to the non-rotating case, but with a slightly smaller $\Delta\nu$[11].

To search for regular patterns we have used observations from the *Transiting Exoplanet Survey Satellite* (*TESS*), which provides light curves for many thousands of δ Scuti stars at rapid cadence (120 s sampling). We used the first nine 27-day sectors of *TESS* data and focussed on identifying δ Scuti stars that pulsate at high frequencies (above about 30 d^{-1}). We also examined stars not previously known to pulsate by calculating the Fourier spectra of *TESS* light curves and measuring the skewness of the distribution of peak heights[12] above 30 d^{-1} as a way to flag likely detections. We then inspected the pulsation spectra for regularity using échelle diagrams (described below). In addition, we used data from the *Kepler* spacecraft, which observed about 300 δ Scuti stars at

short cadence (60 s sampling) during its four-year nominal mission[12–14]. Stars observed in *Kepler*'s long-cadence mode (29.4-min sampling) were not considered because the Nyquist frequency of 24 d^{-1} makes it very difficult to identify patterns in high-frequency pulsators.
We discovered 60 stars with regular frequency spacings (Extended Data Table 1), which define a group of δ Scuti stars for which mode identification is possible. Figure 1 shows some of the pulsation spectra, which have remarkably regular patterns of peaks. The small amplitudes of the highest-frequency modes may indicate that turbulent pressure, rather than the standard opacity mechanism, is responsible for driving them[15]. About one third of the stars in our sample (e.g., bottom half of Fig. 1) show a strong peak in the range 18–23 d^{-1}, which is likely to be the fundamental radial pressure mode ($n = 1$, $l = 0$). This identification is strengthened by the fact that these peaks agree with the established period–luminosity relation for the fundamental radial mode in δ Scuti stars[16], and by the fact that we find a good correlation between this frequency (when present) and the measured value of $\Delta\nu$ (Extended Data Fig. 2). In addition, six stars show a mode that is a factor ~ 0.78 shorter in period, consistent with being the first radial overtone ($n = 2$, $l = 0$)[17].
Figure 2 shows the pulsation spectra of several δ Scuti stars in échelle format, where the spectra have been divided into equal segments of width $\Delta\nu$ and stacked vertically so that peaks with the same degree fall along ridges. The regularity of the patterns is striking, similar to échelle diagrams of solar-like oscillators[1–3] but at much lower radial orders. Comparison with pulsation frequencies calculated from theoretical models (red symbols in the top row) enables an unambiguous identification of ridges corresponding to sequences of radial modes ($l = 0$) and dipolar modes ($l = 1$), as shown (more examples are shown in Extended Data Fig. 1). Sequences of $l = 2$ modes do not appear to be present in these stars.
We have placed our sample in the Hertzsprung–Russell (H–R) diagram using effective temperatures and luminosities derived from broadband colors and *Gaia* parallaxes (Fig. 3a). The δ Scuti stars with regular frequency spacings tend to be located near the zero-age main-sequence (ZAMS), with masses between 1.5 and 1.8 $M_\odot$. The fact that these stars are relatively young helps to explain their regular pulsation spectra. In more evolved stars, the nonradial modes are expected to be "bumped" from their regular spacings when they undergo avoided crossings due to coupling with gravity (buoyancy) modes in the core[3]. For young stars, this mode bumping only occurs at the lowest frequencies, as can be seen from the models of $l = 1$ modes in Fig. 2 (top row; red triangles at low frequencies).
The large frequency separation, $\Delta\nu$, scales approximately as the square root of the mean stellar density[11,18–20]. However, the mode spacings of stars are not completely regular—even in the asymptotic regime—meaning that $\Delta\nu$ varies with frequency. We used theoretical models to calculate $\Delta\nu$ for δ Scuti stars in the same region that we measured it, namely from radial modes with orders in the range $n = 4$ to 8 (see Methods). We found that $\Delta\nu$ in the models was typically 15% lower than would be obtained by scaling from the density of the Sun, which is consistent with previous results[10,18–20]. Figure 3b compares the observed large separations of our sample with the densities derived from fitting to evolutionary tracks in the H–R diagram. The results confirm there is a correlation, with most stars lying between the values based on the standard scaling relation (solid red curve) and those from the model calculations (dashed red curve). Some

of the spread is probably due to the range of metallicities of the sample, and some will be due to rotation. For example, if a star is oblate due to rotation then the mean density will be reduced. In addition, the inclination of its rotation axis affects the observed position in the H–R diagram[21] (and hence the inferred radius, mass and density). The absolute position of the regular comb pattern, parametrised by the phase term ϵ (see Methods), also contains important information about the interior structure of the star. In solar-type stars, the value of ϵ does not change greatly during evolution[22]. In these intermediate-mass stars, this appears not to be the case and ϵ serves as a useful indicator for age (Fig. 3c).

High-resolution spectroscopy can be used to measure the projected rotational velocity of a star, and most intermediate-mass stars have $v \sin i$ values[23] in the range 50–220 km s^{-1}. Measurements are available for 39 of the 60 stars in our sample (see Extended Data Table 2), of which 17 stars have $v \sin i \leq 50$ km s^{-1}. Thus, our sample of δ Scuti stars includes many with unusually low projected rotational velocities, which is consistent with the idea that regular frequency spacings are more common in stars seen at high inclinations (close to pole-on).

Some échelle diagrams show the modes along the $l = 1$ ridge to be split into close doublets, as expected for rotating stars (some examples, namely HD 24975 and HD 46722, are shown in Extended Data Fig. 1). Four échelle diagrams show more complicated patterns, with additional ridges at various angles that indicate sequences with slightly different spacings (Fig. 4). The rotation axes of these stars are presumably at higher inclinations than those with simpler pulsation spectra, which would lead us to expect one $l = 0$ ridge and three $l = 1$ ridges. Beyond the usual rotational splitting of $l = 1$ modes, slightly different frequency spacings are expected for each m in an oblate star. This is because modes with different m propagate along different paths through the star, giving different values for the sound-speed crossing time and hence for $\Delta\nu$. In stars with even more ridges, the additional sequences could correspond to modes with higher degrees ($l \geq 2$)—where coupling between modes with different degree may also be important—and perhaps also to chaotic modes[9,24].

The identification of regular pulsation frequency patterns in intermediate-mass stars will expand the reach of asteroseismology to new frontiers. One example is to determine the ages of young moving groups, clusters, and stellar streams, which can vary by up to a factor of two, depending on the method used[25]. Spectroscopic radial velocities and *Gaia* astrometry show that several stars in our sample are members of nearby young associations (references given in Extended Data Table 1), including the Octans association (HD 44930, HD 29783, HD 42915), the Carina association (HD 89263), the Columba association (HD 37286 = HR 1915), the β Pictoris moving group (β Pic itself) and the recently-discovered Pisces–Eridanus stellar stream (HD 31901). For the latter, gyrochronology yielded an age similar to the Pleiades (~ 130 Myr)[26], in contrast to the initial ~ 1 Gyr age determination from suspected evolved moving group members[27].

Asteroseismic modelling of HD 31901 (Fig. 2c) clearly confirms a young age for this member of the Pisces–Eridanus group (see Methods), and similar age determinations might be possible for other groups containing intermediate-mass stars.

Four stars in our sample (HD 28548, HD 34282, TYC 5945-497-1 and V1790 Ori) exhibit excess emission in the WISE passbands, indicating a circumstellar dust disk. One of these (HD 34282) has a disk that has been resolved by ALMA, showing it to be inclined $60^\circ \pm 1^\circ$ to the line of

sight[28]. The constraints on age and inclination of this host star provided by an analysis of its pulsations could illuminate the origin of stellar obliquity[29] and the pace of disk evolution[30]. Finally, we note that six stars in our sample have been classified spectroscopically as λ Bootis stars (references given in Extended Data Table 1), meaning that their surface chemical abundances show evidence for accretion from circumstellar material. Given that λ Bootis stars are rare, making up only about 2% of A stars[31], the relatively high occurrence rate in our sample lends support to the hypothesis that λ Bootis stars tend to be young, with circumstellar material accreting from a proto-planetary disk.

The stars observed by *TESS* at 2-minute cadence constitute a small fraction of stars that fall on the full-frame images (FFIs). Future *TESS* observations should reveal many more examples of δ Scuti stars with high-frequency overtones, especially given that the cadence of *TESS* FFIs will switch from 30 minutes to 10 minutes in the extended mission that starts in July 2020. It is likely that the stars with regular patterns can guide mode identification in the much larger number of δ Scuti stars whose pulsation spectra are not as regular.

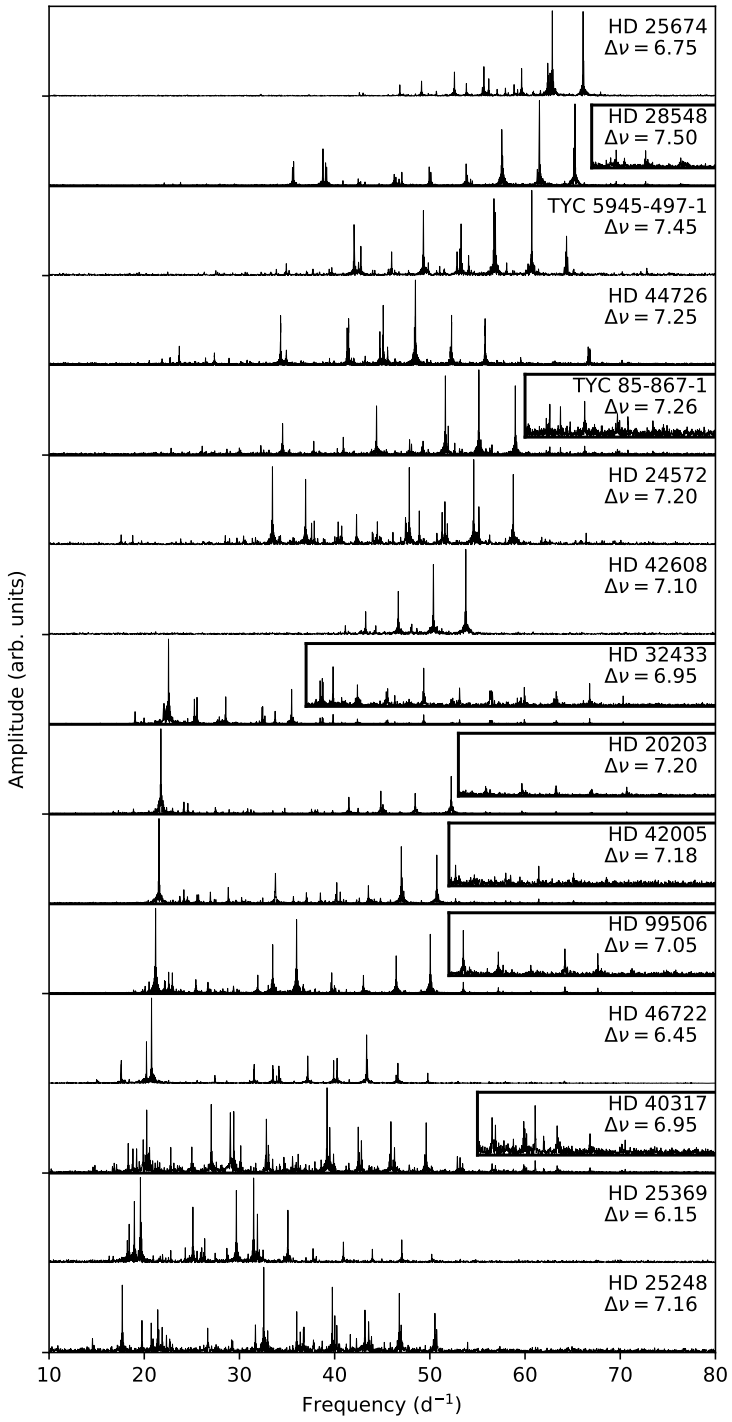

Fig. 1 | Pulsation spectra of 15 high-frequency δ Scuti stars observed with *TESS*. The measured value of $\Delta\nu$ (in d^{-1}) is given in each panel (see Extended Data Table 1). The insets for some stars expand the vertical axis by a factor of 4 to make weaker peaks more visible.

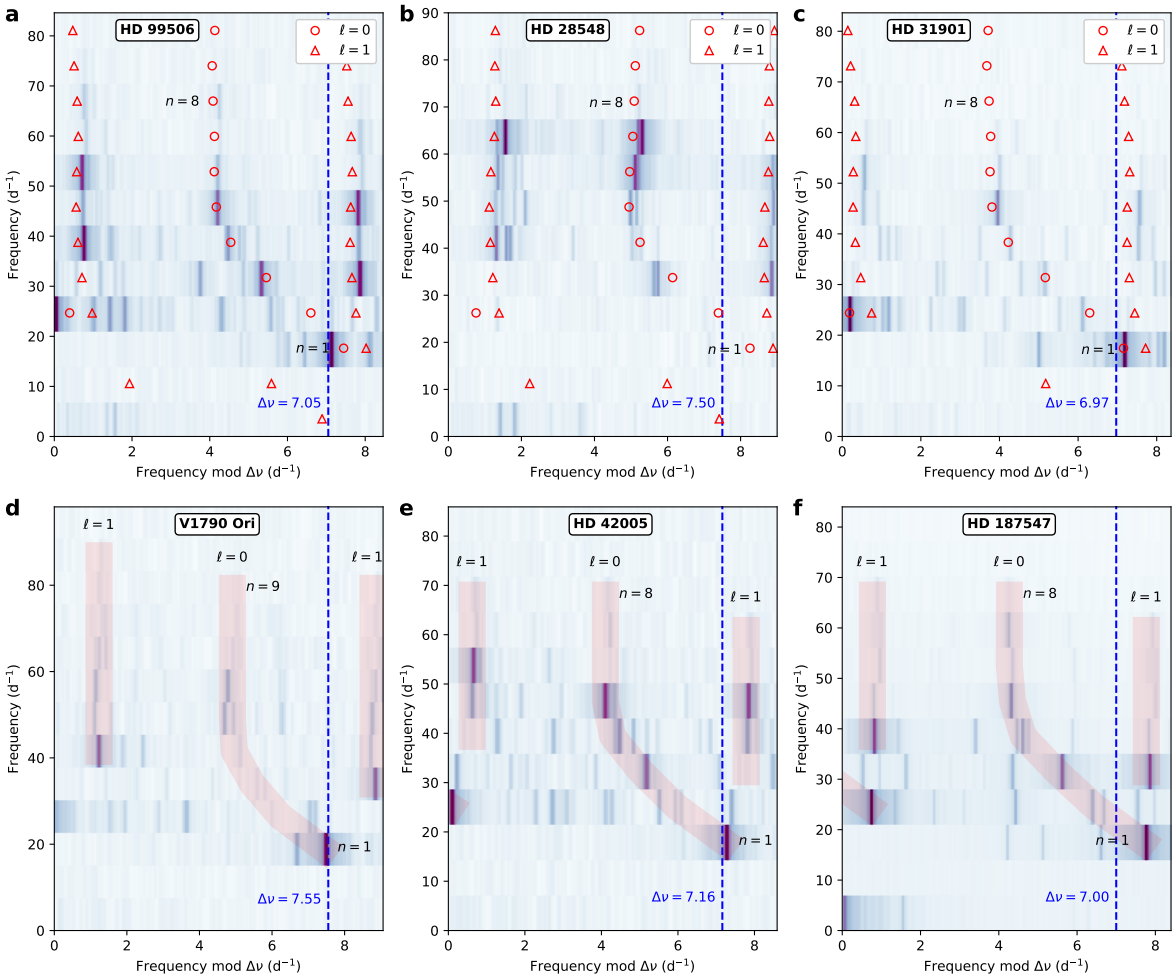

Fig. 2 | Mode identification in δ Scuti stars. The pulsation spectra are shown in échelle format, with segments of equal length being stacked vertically. The vertical dashed line shows the value of $\Delta\nu$ used in each case, with a repeated overlap region added on the right for clarity. The greyscale shows the observed amplitude spectrum, which in most cases is calculated from one 27-day sector of data from the *TESS* spacecraft. The exception is HD 187547, for which observations were made over 960 d with the *Kepler* spacecraft[32]. Some smoothing was applied to the observed amplitude spectra before plotting. In the top row, the red symbols show mode frequencies calculated from theoretical models of non-rotating stars, chosen to match the observed modes reasonably well (see Methods). These allow mode identifications in other stars, as shown in the bottom row, where the red stripes mark overtone sequences of $l = 0$ and $l = 1$ modes. The parameters of the models shown in the top row are as follows (while noting that other values of the parameters also give fits of similar quality): **a,** HD 99506: mass $1.68\,M_\odot$, metallicity [Fe/H] $= 0.0$, age 200 Myr, effective temperature 8065 K and radius $1.51\,R_\odot$. **b,** HD 28548: mass $1.59\,M_\odot$, metallicity [Fe/H] $= -0.2$, age 270 Myr, effective temperature 8202 K and radius $1.41\,R_\odot$. **c,** HD 31901: mass $1.77\,M_\odot$, metallicity [Fe/H] $= 0.08$, age 102 Myr, effective temperature 8083 K and radius $1.51\,R_\odot$.

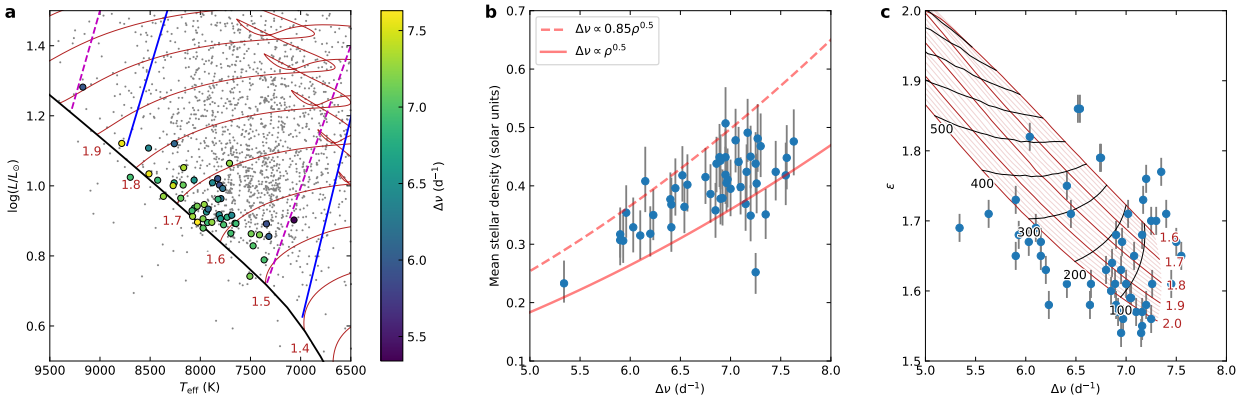

Fig. 3 | Properties of high-frequency δ Scuti stars. a, Location of our sample in the H–R diagram (circles, colour-coded by the measured large-frequency separation). The small points show δ Scuti stars observed by the *Kepler* Mission[12] and the red curves (labelled by mass in solar units) are evolutionary tracks calculated for solar metallicity (see Methods). The solid blue lines show the edges of the theoretical δ Scuti instability strip and the dashed magenta lines show the observed instability strip based on *Kepler* stars[12]. **b,** Mean stellar density versus large-frequency separation as determined from observations (symbols, with 1-σ uncertainties), as predicted from the standard scaling relation (solid red line) and from non-rotating stellar models (red dashed line). Stars with close binary companions have been omitted from panels **a** and **b** (see Methods). **c,** The phase term ϵ, which measures the absolute position of the oscillation spectrum, versus large frequency separation. Symbols show observed values. Red curves (labelled by mass in solar units) are evolutionary tracks based on fitting to radial modes with $n = 4$ to 8 (see Methods), and shorter black curves are the corresponding isochrones, labelled in Myr. These models are only intended to be indicative, since they are calculated for solar metallicity and do not include rotation, which affects both $\Delta\nu$ and ϵ. The models do show that, unlike for solar-type stars[22], ϵ varies significantly during the evolution and is therefore sensitive to age, which is an important bonus for asteroseismology of δ Scuti stars.

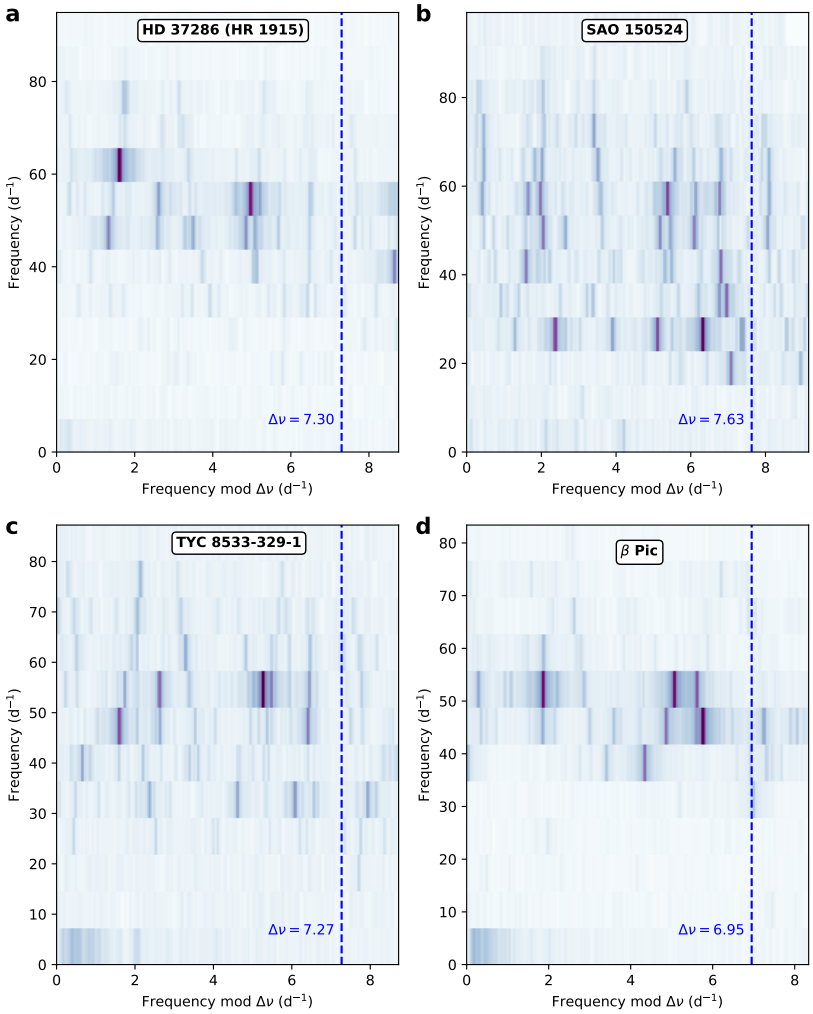

Fig. 4 | Examples of more complicated échelle diagrams of δ Scuti pulsations. There are several sets of ridges at a range of angles, indicating slightly different spacings. An intermediate value of $\Delta\nu$ was chosen for these diagrams (see Methods).

Acknowledgements: We gratefully acknowledge the *TESS* and *Kepler* teams, whose efforts made these results possible. This research was partially conducted during the Exostar19 program at the Kavli Institute for Theoretical Physics at UC Santa Barbara, which was supported in part by the National Science Foundation under Grant No. NSF PHY-1748958. We thank colleagues in that program, especially Rich Townsend, for many stimulating discussions. We also thank Andrés Moya, Antonio García Hernández, Juan Carlos Suárez and Zhao Guo for comments on the manuscript. We gratefully acknowledge support from the Australian Research Council (grant DE 180101104), and from the Danish National Research Foundation (Grant DNRF106) through its funding for the Stellar Astrophysics Center (SAC). D.H. acknowledges support from the Alfred P. Sloan Foundation, the National Aeronautics and Space Administration (80NSSC18K1585, 80NSSC19K0379), and the National Science Foundation (AST-1717000). Y.L. acknowledges the Joint Research Fund in Astronomy (U1631236) under cooperative agreement between the National Natural Science Foundation of China (NSFC) and Chinese Academy of Sciences (CAS). D.L.H. acknowledges support by the Science and Technology Facilities Council under grant ST/M000877/1. The research leading to these results has (partially) received funding from the Research Foundation Flanders (FWO) under grant agreement G0H5416N (ERC Runner Up Project). This work makes use of observations from the LCOGT network. This work has made use of data from the European Space Agency (ESA) mission *Gaia* (`https://www.cosmos.esa.int/gaia`), processed by the *Gaia* Data Processing and Analysis Consortium (DPAC, `https://www.cosmos.esa.int/web/gaia/dpac/consortium`). Some of the observations reported in this paper were obtained with the Southern African Large Telescope (SALT) under programs 2015-2-SCI-007, 2016-2-SCI-015 and 2017-2-SCI-010. The ISIS instrument is mounted on the WHT, which is operated on the island of La Palma by the Isaac Newton Group of Telescopes in the Spanish Observatorio del Roque de los Muchachos of the Instituto de Astrofsica de Canarias. The Veloce Rosso facility was funded by an Australian Research Council (ARC) Linkage Infrastructure, Equipment and Facility (LIEF) grants LE150100087 & LE160100014, and UNSW Research Infrastructure Scheme grant RG163088. CGT and CB acknowledge the support of ARC Discovery grant DP170103491. The authors wish to recognize and acknowledge the very significant cultural role and reverence that the summit of Mauna Kea has always had within the indigenous Hawaiian community; we are most fortunate to have the opportunity to conduct observations from this mountain. We also acknowledge the traditional owners of the land on which the Anglo-Australian Telescope stands, the Gamilaraay people, and pay our respects to elders past, present, and emerging.

Author Contributions: T.R.B, S.J.M., D.R. Hey, W.J.C., G.L., Y.L., I.L.C. and J.Y. analysed the photometric observations; T.L., D.S., W.H.B, T.R.W., D.R.R., J.F. and J.J.H. calculated and/or interpreted theoretical models; V.A. and H.K. coordinated the selection of the targets for the *TESS* observations; D.H., D.R. Harbeck, S.S., B.S., T.M.B., A.W.H., H.I., C.M., M.R., C.B., A.D.R., C.G.T, M.J.I and D.L.H obtained and/or analysed the spectroscopic observations; E.G. and A.M. identified objects that belong to moving groups; G.R.R., R.K.V. and J.M.J. were key architects of the *TESS* Mission. All authors reviewed the manuscript.

Competing Interests: The authors declare no competing interests.

METHODS

Pulsation Analysis. Light curves from *TESS*[33] and *Kepler*[34] were downloaded from MAST (Barbara A. Mikulski Archive for Space Telescopes)[35]. We used the Pre-search Data Conditioning Simple Aperture Photometry (PDCSAP) to calculate the Fourier amplitude spectra using a standard Lomb-Scargle periodogram.

For *TESS*, we examined all 92,000 stars having 2-minute light curves in Sectors 1–9. We used the skewness of the distribution of peak heights[12] above $30\,\mathrm{d}^{-1}$ as a way to identify high-frequency δ Scuti pulsators, producing a list of $\sim$1000 stars. Inspecting their échelle diagrams (see below) revealed 57 δ Scuti stars having a regular series of high-frequency peaks. For *Kepler*, we looked at all $\sim$330 δ Scuti stars that have short-cadence data (60 s sampling) and identified three stars with regular peaks.

The large separations ($\Delta\nu$) for the 60 stars in our sample are listed in Extended Data Table 1. In most cases, $\Delta\nu$ was measured by aligning the highest-frequency radial modes in a vertical ridge in the échelle diagram using the Python package `echelle`[36], which allows the value of $\Delta\nu$ to be fine-tuned interactively. This allowed $\Delta\nu$ to be measured to a precision of about $0.02\,\mathrm{d}^{-1}$ (see examples in Fig. 2 and Extended Data Fig. 1). Four stars do not show a clear sequence of radial modes, with the échelle diagrams showing several ridges that are not quite parallel (Fig. 4). In these cases, we chose $\Delta\nu$ to be the average of the values needed to make the individual ridges vertical.

The phase term ϵ is given for those stars having a clear $l = 0$ sequence, as determined from the horizontal position of that ridge in the échelle diagram. Note that $\Delta\nu$ and ϵ are related to the frequencies of high-order radial modes via the asymptotic relation[1–3]: $\nu_{n,l=0} \approx \Delta\nu(n + \epsilon)$. The uncertainty in ϵ determined in this way is about 0.02.

To rule out contamination from nearby stars as the source of the observed pulsations, we examined the pixel data and cross-matched with the *Gaia* DR2 catalogue. We considered a region of 5×5 TESS pixels (63×63 arcsec) centred on each target. We found that no dilution is present in one third of the targets, with most of the remainder having small amounts of dilution (0.1–3%). Only five stars have dilutions above 8%. We conclude that contamination of the photometry from nearby stars is not significant.

Fundamental Stellar Properties. To estimate properties for our sample we used Tycho B_T and V_T photometry[37], which we transformed into Johnson B and V magnitudes[38]. We then used a $(B - V)$–$T_{\rm eff}$ relation[39], Gaia DR2 parallaxes[40], a 3D dust map[41], and V-band bolometric corrections to calculate effective temperatures and luminosities. We did this by solving for the distance modulus, as implemented in the "direct mode" version of `isoclassify`[42]. For stars with typical uncertainties > 0.01 mag in Tycho ($V_T > 9$ mag) we used Gaia $BP - RP$, with which we interpolated the colour–$T_{\rm eff}$ relation in the MIST (MESA Isochrones and Stellar Tracks) model grid[43] for solar metallicity to derive $T_{\rm eff}$, and used 2MASS K-band magnitudes in combination with Gaia parallaxes to derive luminosities.

We adopted 2% fractional uncertainties for all derived effective temperatures, which is typical of the residual scatter in optical colour-temperature relations[44]. A comparison of our Gaia-derived

temperatures with those derived from Tycho photometry for stars with $V_T < 10$ mag, and a comparison with an independent implementation of the infrared flux method (IRFM), both showed good agreement with no significant systematic offsets. Our effective temperatures are on average $\sim 1.5\%$ (~ 200 K) hotter than those for A-type stars in the *Kepler* Stellar Properties Catalog[45,46], which were predominantly based on the Kepler Input Catalog (KIC)[47]. Such systematic differences are typical for effective temperature scales in A stars, reflecting the fact that the KIC was not optimized for A stars.

To estimate mean stellar densities, we fitted the effective temperatures and luminosities derived in the previous step to MIST isochrones using the "grid mode" of `isoclassify`, assuming a solar-neighborhood metallicity prior. The procedure also yielded estimates of stellar masses and surface gravities, which combined with $T_{\rm eff}$ were used for the interpolation of bolometric corrections in the previous step. We iterated between the "direct mode" and "grid mode" calculations until all values converged, and adopted 0.03 mag bandpass-independent uncertainties in reddening and bolometric corrections. Extended Data Table 1 lists all stellar properties of the sample. Typical uncertainties are ~ 5 % in luminosity and ~ 15 % in mean stellar density. The properties of V1366 Ori (HD 34282) are not shown because they are highly uncertain due to obscuration by circumstellar material (it is classified as a Herbig Ae star)[48]. This star is not plotted in Fig. 3.

To identify close binaries, which could bias the derived stellar parameters, we cross-matched our targets with the Washington Double Star catalogue (WDS). We also calculated the *Gaia* DR2 re-normalized unit weight error (RUWE) for each target, which provides a quality metric that accounts for the effects of colour and apparent magnitude on *Gaia* astrometric solutions. Stars with WDS companions within 2 arcsec or *Gaia* RUWE > 2 do not have parameters in Extended Data Table 1 and were not plotted in Fig. 3.

High-Resolution Spectroscopy. We obtained optical high-dispersion spectra of some stars in the sample in April and May 2019 using the HIRES spectrograph[49] at the Keck-I 10-m telescope on Maunakea observatory, Hawai'i. The spectra were obtained and reduced as part of the California Planet Search queue[50]. We typically obtained 1-minute integrations using the C5 decker, resulting in a S/N per pixel of 50 at ~ 600 nm with a spectral resolution of $R \sim 60000$. High-resolution spectra for some stars were obtained in May and June 2019 using the NRES spectrograph[51] at the Las Cumbres Observatory Global Telescope Network[52] 1-meter telescopes at Cerro Tololo Inter-American Observatory, Chile and Sutherland, South Africa. Exposure times were typically 10 minutes, resulting in a S/N per resolution element above 70 at ~ 510 nm, with a spectral resolution of $R \sim 50000$. High-resolution spectra for an additional 9 stars were obtained in June 2019 using the Veloce Rosso spectrograph[53] at the 3.9-m Anglo-Australian Telescope (AAT). These spectra covered the range 580–930 nm at a resolution of $R \sim 75000$. Typical exposure times were 5–10 minutes (in cloudy conditions), resulting in a S/N per pixel of 50–90 at $\sim$780 nm.

Extended Data Figure 3 shows a small region of some of these spectra, alongside the Fourier amplitude spectra. The spectral analysis was performed using the UCLSYN spectral synthesis package[54,55] using ATLAS9 models without convective overshooting[56]. Atomic data used in the

analysis was obtained from the VALD database[57], using their default search and extraction parameters. Surface gravities were fixed to $\log g = 4.0$ for all stars in the analysis. A microturbulence velocity of $\xi = 3\,\mathrm{km\,s^{-1}}$ was assumed, which is the typical value for stars within the spectral range considered here[58,59]. Measurements of the projected equatorial rotation velocity ($v \sin i$) were obtained through individual fits to several small (5 nm) regions between 500 nm and 550 nm (and 620–650 nm plus 778 nm for the AAT spectra), avoiding any inter-order gaps. The final values were determined by calculating the mean and sample deviation of the values obtained in the small spectral regions.

An independent set of $v \sin i$ values were determined for 5 of the spectra using the Grid Search in Stellar Parameters (GSSP) software[60]. GSSP is designed to fit a grid of synthetic spectra with varying $T_{\rm eff}$, $\log\ g$, ξ, $v \sin i$ and $[M/H]$ to each observed spectrum and output the χ^2 values of the fit. These synthetic spectra are generated on-the-fly during the fitting process using the SYNTHV radiative transfer code[61] combined with a grid of atmospheric models from the LLMODELS code[62]. We fixed the microturbulent velocity at $\xi = 2.0\,\mathrm{km\,s^{-1}}$ to prevent degeneracies with metallicity. The derived values were found to agree within uncertainties with the results from the UCLSYN spectral synthesis.

For a further 9 stars, we estimated $v \sin i$ using low-resolution spectra that were obtained either with the RSS instrument on the Southern African Large Telescope (SALT)[63–65] or the ISIS instrument on the William Herschel Telescope (WHT). Exposure times were typically a few minutes, which provided a S/N of ~ 100 at a spectral resolution of $R \sim 3000$. For each target, a coarse grid of synthetic models was constructed using the stellar parameters in Extended Data Table 1 and a range of $v \sin i$ values. The observations were compared to the synthetic spectra to estimate the $v \sin i$ and the associated uncertainty.

Extended Data Table 2 lists the determined $v \sin i$ values for each star. Values in parentheses indicate close binaries (see above), meaning that $v \sin i$ may not be reliable.

To determine membership of moving groups, clusters and stellar streams, we calculated barycentric radial velocities using the Python implementation `barycorrPy`[66] of the barycentric correction algorithm of Wright et al. (2014)[67]. These were combined with space motions calculated from *Gaia* DR2 astrometry, and Bayesian posterior probabilities of membership in known nearby moving groups were calculated using `Banyan` Σ[68].

Stellar Models. The stellar models presented in Fig. 2 used the 'astero' extension of MESA (Modules for Experiments in Stellar Astrophysics)[69–71]. We used two approaches that gave similar results. One was based on a model grid calculated with MESA (v8118), where we varied mass from 1.3 to 1.9 $M_\odot$ in steps of 0.01 $M_\odot$ and metallicity ([Fe/H]) from -0.5 to 0.5 in steps of 0.1. We used a fixed (solar-calibrated) mixing-length parameter of $\alpha_{\rm MLT}$ = 1.9 and a helium-to-heavy-element enrichment ratio of 1.33. The best-fitting model was found by Maximum Likelihood Estimation, where we included effective temperature, metallicity, luminosity and all identified pulsation frequencies. Equal weight was given in the likelihood function to the following five observables: frequencies of radial modes, frequencies of dipolar modes, effective temperature, metallicity and luminosity. The other approach used the automated simplex search in MESA-astero (v7503), where the fit was guided by the observed radial modes

only. The search was allowed to vary the mass, metallicity, mixing length, and the age of the model in order to converge to the best fit. A helium-to-heavy-element enrichment ratio of 1.4 was used. Both approaches assumed a primordial helium abundance of 0.249 and we did not make any correction for surface effects in the way that is commonly done for solar-like stars[72].
For the three examples shown in Fig. 2 (upper row), the agreement between models and observations is sufficiently good that we can unambiguously identify the two sequences corresponding to $l = 0$ and $l = 1$ modes. One noteworthy feature of the models and the observations is that the $l = 0$ sequence bends to the right at the bottom of each figure, indicating that $\Delta\nu$ decreases towards the lowest-order modes, whereas the $l = 1$ sequence does not show this effect. This difference is a general feature of these models and makes it possible to identify the sequences in other stars, as shown in Fig. 2 (lower row) and Extended Data Fig. 1.
For Fig. 3a we used the evolutionary tracks with solar metallicity ($X = 0.71$, $Z = 0.014$) from Murphy et al. (2019)[12]. The other parameters of those tracks are $\alpha_{\rm MLT} = 1.8$, exponential core overshooting of 0.015 H_p (pressure scale heights), exponential over- and undershooting of 0.015 H_p for the hydrogen-burning shell, exponential envelope overshooting of 0.025 H_p, diffusive mixing $\log D_{\rm mix} = 0$ (in cm^{2}s^{-1}), OPAL opacities, and the solar abundance mixture[73]. As noted by Murphy et al. (2019), these tracks are in good agreement with the MIST tracks computed with no rotation and similar metallicities, except that the former have a longer main-sequence phase. This is not expected to be important for our targets, which are mostly young (close to the ZAMS). Although it is possible for δ Scuti pulsations to occur in the pre-main-sequence (PMS) phase, prior to the onset of hydrogen burning[74], there is no indication of a PMS classification in the literature for most of the stars in our sample.

Detailed modelling of HD 31901. As a member of the Pisces–Eridanus stellar stream, this star makes a good test case. We used the models described above, constrained by the observed frequencies of the radial and dipole modes and by the observed effective temperature and luminosity. Following Curtis et al. (2019)[26], we assumed the metallicity is close to solar. The results imply a mass of $1.71 \pm 0.05\,M_\odot$, a radius of $1.54 \pm 0.03\,R_\odot$ and an age of 150 ± 100 Myr. The latter is consistent with the age of $\sim$130 Myr from Curtis et al. (2019)[26] but not with the value of ~ 1 Gyr determined by Meingast et al. (2019)[27].

Additional references and notes on individual stars. As mentioned in the main text, several previous studies have reported regular frequency spacings in the Fourier amplitude spectra of δ Scuti stars[14,18–20,48,75–86]. Among these, the following stars are included in our sample:

- HD 187547 (KIC 7548479): the large frequency spacing was previously reported as 40.5 μHz (3.5 d^{-1})[32,79], which is factor of two smaller than the value we have identified from the same *Kepler* observations. Comparing the échelle diagram of this star (Fig. 2) with others in our sample indicates that the larger $\Delta\nu$ is correct. This is also consistent with the *Gaia* DR2 parallax (6.57 ± 0.24 mas), which places this star close to the ZAMS.

- HD 34282 (V1366 Ori): based on observations with MOST (Microvariability and Oscillations of Stars), Casey et al. (2013)[48] reported a large separation of 3.75 d^{-1}, which is

half the value reported here. Both values would be consistent with the HIPPARCOS parallax (5.24 ± 1.67 mas), as used by Casey et al., but the much more precise *Gaia* DR2 parallax (3.08 ± 0.29 mas) and comparison with other stars in our sample confirms that the larger $\Delta\nu$ value is correct. V1366 Ori is a Herbig Ae star[87], so it may be pre-main-sequence. Its classification in SIMBAD as an eclipsing binary appears to be incorrect.

- β Pictoris: known to be a high-frequency δ Scuti star[88,89], but a value for the large separation has not been reported. The TESS observations indicate a value of $\Delta\nu = 6.95\,\mathrm{d}^{-1}$ (Fig. 4).

The following stars are not in our sample but seem likely to be high-frequency δ Scuti stars with regular spacings:

- HD 144277: based on data from MOST and CoRoT (COnvection, ROtation and planetary Transits), Zwintz et al. (2011)[80] suggested a large separation of $7.2\,\mathrm{d}^{-1}$. This star will not be observed by *TESS* in its nominal two-year mission[90]

- HD 261711: based on MOST and CoRoT data, Zwintz et al. (2013)[81] suggested a large separation of $6.72\,\mathrm{d}^{-1}$. This star was observed by *TESS* in Sector 6, but only with 30-minute sampling.

- HD 174966: based on CoRoT data, García Hernández et al. (2013)[83] suggested a large separation of $5.53\,\mathrm{d}^{-1}$. This star will not be observed by *TESS* in its nominal two-year mission[90].

- XX Pyx: based on ground-based multisite observations, Handler et al. (2000)[75] reported 22 pulsation frequencies in the range 27 to $76\,\mathrm{d}^{-1}$, and suggest a large separation of $4.63\,\mathrm{d}^{-1}$. We have examined the published frequencies for this star using échelle diagrams and confirm that a value of $\Delta\nu = 4.70\,\mathrm{d}^{-1}$ gives a reasonably good alignment of the peaks. This star will not be observed by *TESS* in its nominal two-year mission[90].

- HD 156623: based on observations with the bRing robotic observatory network, Mellon et al. (2019)[91] found frequencies in the range 60–$70\,\mathrm{d}^{-1}$ and suggested regularity at three different separations: 3.75, 7.25, and $2.75\mathrm{d}^{-1}$. This star was observed by TESS in Sector 12 and shows a pattern similar to other stars in our sample, with a spacing of $\Delta\nu = 7.31\,\mathrm{d}^{-1}$.

- HD 27462 (TT Ret): based on *TESS* data, Khalack et al.[92] preferred a large separation of $3.3\,\mathrm{d}^{-1}$. Our examination of the *TESS* data and a comparison with the stars in our sample suggests $\Delta\nu = 6.9\,\mathrm{d}^{-1}$. The WDS catalog[93] lists this star as a binary with a separation of 0.4 arcsec and a magnitude difference of 0.7. This is consistent with Gaia DR2, which gives no parallax and a large astrometric excess noise (RUWE ~ 77). Accounting for the binary, the HIPPARCOS parallax places the two components close to the ZAMS, consistent with our suggested value of $\Delta\nu$.

Data Availability. *TESS* and *Kepler* data are available from the MAST portal at https://archive.stsci.edu/access-mast-data. All other data are available from the corresponding author upon reasonable request.

Code Availability. We have made use of standard data analysis tools in Python, as noted and referenced in Methods.

1. Aerts, C., Christensen-Dalsgaard, J. & Kurtz, D. W. *Asteroseismology* (Springer, 2010).

2. García, R. A. & Ballot, J. Asteroseismology of solar-type stars. *Living Reviews in Solar Physics* **16**, 4 (2019).

3. Hekker, S. & Christensen-Dalsgaard, J. Giant star seismology. *Astron. Astrophys. Rev.* **25**, 1 (2017).

4. Aerts, C. Massive Star Asteroseismology in Action. In Meynet, G., Georgy, C., Groh, J. & Stee, P. (eds.) *New Windows on Massive Stars*, vol. 307 of *IAU Symposium*, 154–164 (2015).

5. Córsico, A. H., Althaus, L. G., Miller Bertolami, M. M. & Kepler, S. O. Pulsating white dwarfs: new insights. *Astron. Astrophys. Rev.* **27**, 7 (2019).

6. Goupil, M. J. *et al.* Asteroseismology of δ Scuti Stars: Problems and Prospects. *J. Astron. Astrophys.* **26**, 249–259 (2005).

7. Handler, G. Delta Scuti Variables. In Guzik, J. A. & Bradley, P. A. (eds.) *American Institute of Physics Conference Series*, vol. 1170, 403–409 (2009).

8. Ouazzani, R. M., Roxburgh, I. W. & Dupret, M. A. Pulsations of rapidly rotating stars. II. Realistic modelling for intermediate-mass stars. *Astron. Astrophys.* **579**, A116 (2015).

9. Reese, D. R. *et al.* Frequency regularities of acoustic modes and multi-colour mode identification in rapidly rotating stars. *Astron. Astrophys.* **601**, A130 (2017).

10. Mirouh, G. M., Angelou, G. C., Reese, D. R. & Costa, G. Mode classification in fast-rotating stars using a convolutional neural network: model-based regular patterns in δ Scuti stars. *Mon. Not. R. Astron. Soc.* **483**, L28–L32 (2019).

11. Reese, D., Lignières, F. & Rieutord, M. Regular patterns in the acoustic spectrum of rapidly rotating stars. *Astron. Astrophys.* **481**, 449–452 (2008).

12. Murphy, S. J., Hey, D., Van Reeth, T. & Bedding, T. R. Gaia-derived luminosities of Kepler A/F stars and the pulsator fraction across the δ Scuti instability strip. *Mon. Not. R. Astron. Soc.* **485**, 2380–2400 (2019).

13. Balona, L. A., Daszyńska-Daszkiewicz, J. & Pamyatnykh, A. A. Pulsation frequency distribution in δ Scuti stars. *Mon. Not. R. Astron. Soc.* **452**, 3073–3084 (2015).

14. Bowman, D. M. & Kurtz, D. W. Characterizing the observational properties of δ Sct stars in the era of space photometry from the Kepler mission. *Mon. Not. R. Astron. Soc.* **476**, 3169–3184 (2018).

15. Antoci, V. *et al.* The first view of δ Scuti and γ Doradus stars with the TESS mission. *Mon. Not. R. Astron. Soc.* **490**, 4040–4059 (2019).

16. Ziaali, E., Bedding, T. R., Murphy, S. J., Van Reeth, T. & Hey, D. R. The period-luminosity relation for δ Scuti stars using Gaia DR2 parallaxes. *Mon. Not. R. Astron. Soc.* **486**, 4348–4353 (2019).

17. Petersen, J. O. & Christensen-Dalsgaard, J. Pulsation models of δ Scuti variables. I. The high-amplitude double-mode stars. *Astron. Astrophys.* **312**, 463–474 (1996).

18. Suárez, J. C. *et al.* Measuring mean densities of δ Scuti stars with asteroseismology. Theoretical properties of large separations using TOUCAN. *Astron. Astrophys.* **563**, A7 (2014).

19. García Hernández, A. *et al.* Observational $\Delta\nu$-ρ Relation for δ Sct Stars using Eclipsing Binaries and Space Photometry. *Astrophys. J.* **811**, L29 (2015).

20. Paparó, M., Benkő, J. M., Hareter, M. & Guzik, J. A. Unexpected Series of Regular Frequency Spacing of δ Scuti Stars in the Non-asymptotic Regime. II. Sample-Echelle Diagrams and Rotation. *Astrophys. J. Suppl. Ser.* **224**, 41 (2016).

21. Suárez, J. C. *et al.* A study of correlation between the oscillation amplitude and stellar parameters of delta Scutis in open clusters. Toward selection rules for delta Scuti star oscillations. *Astron. Astrophys.* **390**, 523–531 (2002).

22. White, T. R. *et al.* Calculating Asteroseismic Diagrams for Solar-like Oscillations. *Astrophys. J.* **743**, 161 (2011).

23. Zorec, J. & Royer, F. Rotational velocities of A-type stars. IV. Evolution of rotational velocities. *Astron. Astrophys.* **537**, A120 (2012).

24. Evano, B., Lignières, F. & Georgeot, B. Regularities in the spectrum of chaotic p-modes in rapidly rotating stars. *Astron. Astrophys.* **631**, A140 (2019).

25. Mamajek, E. E. & Bell, C. P. M. On the age of the β Pictoris moving group. *Mon. Not. R. Astron. Soc.* **445**, 2169–2180 (2014).

26. Curtis, J. L., Agüeros, M. A., Mamajek, E. E., Wright, J. T. & Cummings, J. D. TESS Reveals that the Nearby PiscesEridanus Stellar Stream is only 120 Myr Old. *Astron. J.* **158**, 77 (2019).

27. Meingast, S., Alves, J. & Fürnkranz, V. Extended stellar systems in the solar neighborhood. II. Discovery of a nearby 120 degree stellar stream in Gaia DR2. *Astron. Astrophys.* **622**, L13 (2019).

28. van der Plas, G. *et al.* An 80 au cavity in the disk around HD 34282. *Astron. Astrophys.* **607**, A55 (2017).

29. Lai, D. Star-disc-binary interactions in protoplanetary disc systems and primordial spin-orbit misalignments. *Mon. Not. R. Astron. Soc.* **440**, 3532–3544 (2014).

30. Williams, J. P. & Cieza, L. A. Protoplanetary Disks and Their Evolution. *Ann. Rev. Astron. Astrophys.* **49**, 67–117 (2011).

31. Paunzen, E. A spectroscopic survey for lambda Bootis stars. III. Final results. *Astron. Astrophys.* **373**, 633–640 (2001).

32. Antoci, V. *et al.* The Role of Turbulent Pressure as a Coherent Pulsational Driving Mechanism: The Case of the δ Scuti Star HD 187547. *Astrophys. J.* **796**, 118 (2014).

33. Ricker, G. R. *et al.* Transiting Exoplanet Survey Satellite (TESS). *J. Astron. Telescopes, Instruments, and Systems* **1**, 014003 (2015).

34. Borucki, W. J. *et al.* Kepler Planet-Detection Mission: Introduction and First Results. *Science* **327**, 977 (2010).

35. `https://mast.stsci.edu/portal/Mashup/Clients/Mast/Portal.html`

36. Daniel R, H. Echelle: Dynamic echelle diagrams for asteroseismology (2020). URL `https://doi.org/10.5281/zenodo.3629933`

37. Høg, E. *et al.* The Tycho-2 catalogue of the 2.5 million brightest stars. *Astron. Astrophys.* **355**, L27–L30 (2000).

38. Bessell, M. S. The Hipparcos and Tycho Photometric System Passbands. *Pub. Astron. Soc. Pac.* **112**, 961–965 (2000).

39. Flower, P. J. Transformations from Theoretical Hertzsprung-Russell Diagrams to Color-Magnitude Diagrams: Effective Temperatures, B-V Colors, and Bolometric Corrections. *Astrophys. J.* **469**, 355–365 (1996).

40. Lindegren, L. *et al.* Gaia Data Release 2. The astrometric solution. *Astron. Astrophys.* **616**, A2 (2018).

41. Bovy, J., Rix, H.-W., Green, G. M., Schlafly, E. F. & Finkbeiner, D. P. On Galactic Density Modeling in the Presence of Dust Extinction. *Astrophys. J.* **818**, 130 (2016).

42. Huber, D. *et al.* The K2 Ecliptic Plane Input Catalog (EPIC) and Stellar Classifications of 138,600 Targets in Campaigns 1-8. *Astrophys. J.* **224**, 2 (2017).

43. Choi, J. *et al.* Mesa Isochrones and Stellar Tracks (MIST). I. Solar-scaled Models. *Astrophys. J.* **823**, 102 (2016).

44. Casagrande, L. *et al.* New constraints on the chemical evolution of the solar neighbourhood and Galactic disc(s). Improved astrophysical parameters for the Geneva-Copenhagen Survey. *Astron. Astrophys.* **530**, A138 (2011).

45. Huber, D. *et al.* Revised Stellar Properties of Kepler Targets for the Quarter 1-16 Transit Detection Run. *Astrophys. J. Suppl. Ser.* **211**, 2 (2014).

46. Mathur, S. *et al.* Revised Stellar Properties of Kepler Targets for the Q1-17 (DR25) Transit Detection Run. *Astrophys. J. Suppl. Ser.* **229**, 30 (Erratum: ApJS, 234, 43) (2017).

47. Brown, T. M., Latham, D. W., Everett, M. E. & Esquerdo, G. A. Kepler Input Catalog: Photometric Calibration and Stellar Classification. *Astron. J.* **142**, 112 (2011).

48. Casey, M. P. *et al.* MOST observations of the Herbig Ae δ-Scuti star HD 34282. *Mon. Not. R. Astron. Soc.* **428**, 2596–2604 (2013).

49. Vogt, S. S. *et al.* HIRES: the high-resolution echelle spectrometer on the Keck 10-m Telescope. In Crawford, D. L. & Craine, E. R. (eds.) *Society of Photo-Optical Instrumentation Engineers (SPIE) Conference Series*, vol. 2198, 362 (1994).

50. Howard, A. W. *et al.* The California Planet Survey. I. Four New Giant Exoplanets. *Astrophys. J.* **721**, 1467–1481 (2010).

51. Siverd, R. J. *et al.* NRES: the network of robotic echelle spectrographs. In *Ground-based and Airborne Instrumentation for Astronomy VII*, vol. 10702 of *Society of Photo-Optical Instrumentation Engineers (SPIE) Conference Series*, 107026C (2018).

52. Brown, T. M. *et al.* Las Cumbres Observatory Global Telescope Network. *Pub. Astron. Soc. Pac.* **125**, 1031 (2013).

53. Gilbert, J. *et al.* Veloce Rosso: Australia's new precision radial velocity spectrograph. In *Proc. S.P.I.E*, vol. 10702 of *Society of Photo-Optical Instrumentation Engineers (SPIE) Conference Series*, 107020Y (2018).

54. Smith, K. C. & Dworetsky, M. M. Report for Workshop on Elemental Abundances Analyses. In Adelman, S. J. & Lanz, T. (eds.) *Elemental Abundance Analyses*, 32 (1988).

55. Smith, K. C. *The chemical compositions of mercury-manganese stars from ultraviolet spectra*. Ph.D. thesis, University of London, University College London, United Kingdom (1992).

56. Castelli, F., Gratton, R. G. & Kurucz, R. L. Notes on the convection in the ATLAS9 model atmospheres. *Astron. Astrophys.* **318**, 841–869 (1997).

57. Kupka, F., Piskunov, N., Ryabchikova, T. A., Stempels, H. C. & Weiss, W. W. VALD-2: Progress of the Vienna Atomic Line Data Base. *Astron. Astrophys. Suppl. Ser.* **138**, 119–133 (1999).

58. Niemczura, E. *et al.* Spectroscopic survey of Kepler stars. I. HERMES/Mercator observations of A- and F-type stars. *Mon. Not. R. Astron. Soc.* **450**, 2764–2783 (2015).

59. Niemczura, E. *et al.* Spectroscopic survey of Kepler stars - II. FIES/NOT observations of A- and F-type stars. *Mon. Not. R. Astron. Soc.* **470**, 2870–2889 (2017).

60. Tkachenko, A. Grid search in stellar parameters: a software for spectrum analysis of single stars and binary systems. *Astron. Astrophys.* **581**, A129 (2015).

61. Tsymbal, V. STARSP: A Software System For the Analysis of the Spectra of Normal Stars. In Adelman, S. J., Kupka, F. & Weiss, W. W. (eds.) *M.A.S.S., Model Atmospheres and Spectrum Synthesis*, vol. 108 of *Astronomical Society of the Pacific Conference Series*, 198 (1996).

62. Shulyak, D., Tsymbal, V., Ryabchikova, T., Stütz, C. & Weiss, W. W. Line-by-line opacity stellar model atmospheres. *Astron. Astrophys.* **428**, 993–1000 (2004).

63. Burgh, E. B. *et al.* Prime Focus Imaging Spectrograph for the Southern African Large Telescope: optical design. In Iye, M. & Moorwood, A. F. M. (eds.) *Instrument Design and Performance for Optical/Infrared Ground-based Telescopes*, vol. 4841 of *Proc. S.P.I.E*, 1463–1471 (2003).

64. Kobulnicky, H. A. *et al.* Prime focus imaging spectrograph for the Southern African large telescope: operational modes. In Iye, M. & Moorwood, A. F. M. (eds.) *Instrument Design and Performance for Optical/Infrared Ground-based Telescopes*, vol. 4841 of *Proc. S.P.I.E*, 1634–1644 (2003).

65. Buckley, D. A. H., Swart, G. P. & Meiring, J. G. Completion and commissioning of the Southern African Large Telescope. In *Society of Photo-Optical Instrumentation Engineers (SPIE) Conference Series*, vol. 6267 of *Proc. S.P.I.E*, 62670Z (2006).

66. Kanodia, S. & Wright, J. Python leap second management and implementation of precise barycentric correction (barycorrpy). *Research Notes of the AAS* **2**, 4 (2018).

67. Wright, J. T. & Eastman, J. D. Barycentric Corrections at 1 cm s^{-1} for Precise Doppler Velocities. *Pub. Astron. Soc. Pac.* **126**, 838–852 (2014).

68. Gagné, J. *et al.* BANYAN. XI. The BANYAN Σ Multivariate Bayesian Algorithm to Identify Members of Young Associations with 150 pc. *Astrophys. J.* **856**, 23 (2018).

69. Paxton, B. *et al.* Modules for Experiments in Stellar Astrophysics (MESA). *Astrophys. J. Suppl. Ser.* **192**, 3 (2011).

70. Paxton, B. *et al.* Modules for Experiments in Stellar Astrophysics (MESA): Planets, Oscillations, Rotation, and Massive Stars. *Astrophys. J. Suppl. Ser.* **208**, 4 (2013).

71. Paxton, B. *et al.* Modules for Experiments in Stellar Astrophysics (MESA): Binaries, Pulsations, and Explosions. *Astrophys. J. Suppl. Ser.* **220**, 15 (2015).

72. Ball, W. H. & Gizon, L. A new correction of stellar oscillation frequencies for near-surface effects. *Astron. Astrophys.* **568**, A123 (2014).

73. Asplund, M., Grevesse, N., Sauval, A. J. & Scott, P. The Chemical Composition of the Sun. *Ann. Rev. Astron. Astrophys.* **47**, 481–522 (2009).

74. Zwintz, K. *et al.* Echography of young stars reveals their evolution. *Science* **345**, 550–553 (2014).

75. Handler, G. *et al.* Delta Scuti Network observations of XX Pyx: detection of 22 pulsation modes and of short-term amplitude and frequency variations. *Mon. Not. R. Astron. Soc.* **318**, 511–525 (2000).

76. García Hernández, A. *et al.* Asteroseismic analysis of the CoRoT δ Scuti star HD 174936. *Astron. Astrophys.* **506**, 79–83 (2009).

77. Breger, M., Lenz, P. & Pamyatnykh, A. A. Towards mode selection in δ Scuti stars: regularities in observed and theoretical frequency spectra. *Mon. Not. R. Astron. Soc.* **396**, 291–298 (2009).

78. Breger, M. *et al.* Regularities in frequency spacings of δ Scuti stars: the Kepler star KIC 9700322. *Mon. Not. R. Astron. Soc.* **414**, 1721–1731 (2011).

79. Antoci, V. *et al.* The excitation of solar-like oscillations in a δSct star by efficient envelope convection. *Nature* **477**, 570–573 (2011).

80. Zwintz, K. *et al.* Regular frequency patterns in the classical δ Scuti star HD 144277 observed by the MOST satellite. *Astron. Astrophys.* **533**, A133 (2011).

81. Zwintz, K. *et al.* Regular frequency patterns in the young δ Scuti star HD 261711 observed by the CoRoT and MOST satellites. *Astron. Astrophys.* **552**, A68 (2013).

82. Paparó, M. *et al.* CoRoT 102749568: mode identification in a δ Scuti star based on regular spacings. *Astron. Astrophys.* **557**, A27 (2013).

83. García Hernández, A. *et al.* An in-depth study of HD 174966 with CoRoT photometry and HARPS spectroscopy. Large separation as a new observable for δ Scuti stars. *Astron. Astrophys.* **559**, A63 (2013).

84. Maceroni, C. *et al.* KIC 3858884: a hybrid δ Scuti pulsator in a highly eccentric eclipsing binary. *Astron. Astrophys.* **563**, A59 (2014).

85. Paparó, M., Benkő, J. M., Hareter, M. & Guzik, J. A. Unexpected Series of Regular Frequency Spacing of δ Scuti Stars in the Non-asymptotic Regime. I. The Methodology. *Astrophys. J.* **822**, 100 (2016).

86. Michel, E. *et al.* What CoRoT tells us about δ Scuti stars. Existence of a regular pattern and seismic indices to characterize stars. In *EPJWC*, vol. 160, 03001 (2017).

87. Mora, A. *et al.* EXPORT: Spectral classification and projected rotational velocities of Vega-type and pre-main sequence stars. *Astron. Astrophys.* **378**, 116–131 (2001).

88. Mékarnia, D. *et al.* The δ Scuti pulsations of β Pictoris as observed by ASTEP from Antarctica. *Astron. Astrophys.* **608**, L6 (2017).

89. Zwintz, K. *et al.* Revisiting the pulsational characteristics of the exoplanet host star β Pictoris. *Astron. Astrophys.* **627**, A28 (2019).

90. `https://heasarc.gsfc.nasa.gov/cgi-bin/tess/webtess/wtv.py`

91. Mellon, S. N. *et al.* Bright Southern Variable Stars in the bRing Survey. *Astrophys. J. Suppl. Ser.* **244**, 15 (2019).

92. Khalack, V. *et al.* Rotational and pulsational variability in the TESS light curve of HD 27463. *Mon. Not. R. Astron. Soc.* **490**, 2102–2111 (2019).

93. Mason, B. D., Wycoff, G. L., Hartkopf, W. I., Douglass, G. G. & Worley, C. E. The 2001 US Naval Observatory Double Star CD-ROM. I. The Washington Double Star Catalog. *Astron. J.* **122**, 3466–3471 (2001).

94. Gray, R. O. *et al.* The Discovery of λ Bootis Stars: The Southern Survey I. *Astron. J.* **154**, 31 (2017).

95. Holdsworth, D. L. *et al.* High-frequency A-type pulsators discovered using SuperWASP. *Mon. Not. R. Astron. Soc.* **439**, 2078–2095 (2014).

96. Rodríguez, E., López-González, M. J. & López de Coca, P. A revised catalogue of delta Sct stars. *Astron. Astrophys. Suppl. Ser.* **144**, 469–474 (2000).

97. Murphy, S. J. *et al.* An Evaluation of the Membership Probability of 212 λ Boo Stars. I. A Catalogue. *Pub. Astron. Soc. Aust.* **32**, e036 (2015).

98. Amado, P. J. *et al.* The pre-main-sequence star HD34282: a very short-period δ Scuti-type pulsator. *Mon. Not. R. Astron. Soc.* **352**, L11–L15 (2004).

99. Zuckerman, B., Rhee, J. H., Song, I. & Bessell, M. S. The Tucana/Horologium, Columba, AB Doradus, and Argus Associations: New Members and Dusty Debris Disks. *Astrophys. J.* **732**, 61 (2011).

100. Torres, C. A. O. *et al.* Search for associations containing young stars (SACY). I. Sample and searching method. *Astron. Astrophys.* **460**, 695–708 (2006).

101. Murphy, S. J. & Lawson, W. A. New low-mass members of the Octans stellar association and an updated 30-40 Myr lithium age. *Mon. Not. R. Astron. Soc.* **447**, 1267–1281 (2015).

102. Paunzen, E. *et al.* λ Bootis stars in the SuperWASP survey. *Mon. Not. R. Astron. Soc.* **453**, 1241–1248 (2015).

103. Bell, C. P. M., Mamajek, E. E. & Naylor, T. A self-consistent, absolute isochronal age scale for young moving groups in the solar neighbourhood. *Mon. Not. R. Astron. Soc.* **454**, 593–614 (2015).

104. Royer, F., Zorec, J. & Gómez, A. E. Rotational velocities of A-type stars. III. Velocity distributions. *Astron. Astrophys.* **463**, 671–682 (2007).

105. Royer, F., Grenier, S., Baylac, M. O., Gómez, A. E. & Zorec, J. Rotational velocities of A-type stars in the northern hemisphere. II. Measurement of v sin i. *Astron. Astrophys.* **393**, 897–911 (2002).

106. Schröder, C., Reiners, A. & Schmitt, J. H. M. M. Ca II HK emission in rapidly rotating stars. Evidence for an onset of the solar-type dynamo. *Astron. Astrophys.* **493**, 1099–1107 (2009).

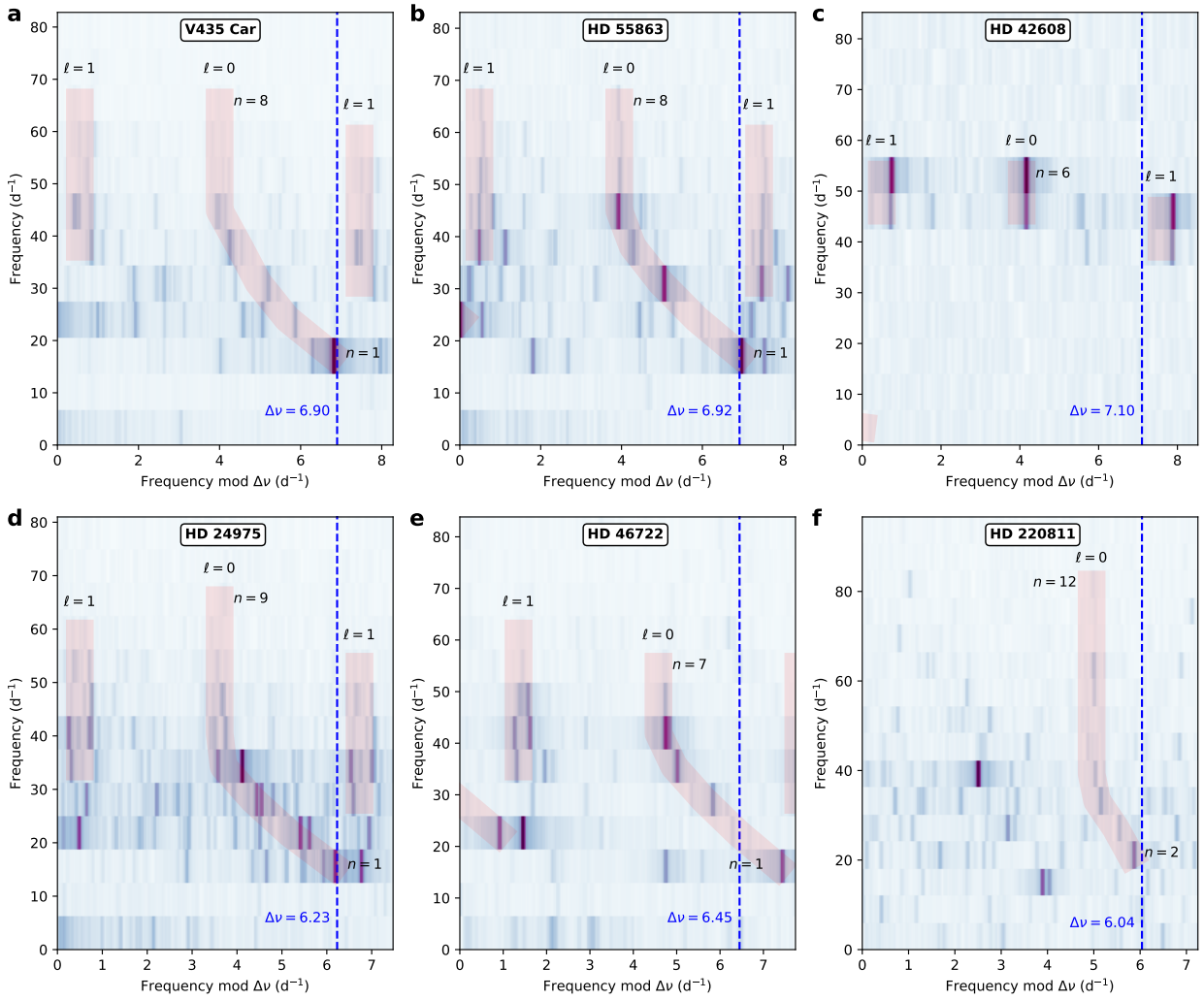

Extended Data Fig. 1 | More examples of mode identifications in δ Scuti stars. The amplitude spectra are shown in échelle format, with segments of equal length being stacked vertically. The vertical dashed line shows the value of $\Delta\nu$ used in each case, with a repeated overlap region added on the right for clarity. The greyscale shows the observed amplitude spectrum of data from the *TESS* spacecraft, where the number of 27-day sectors was four for V435 Car, three for HD 55863, two for HD 24975 and HD 46722, and one for HD 42608 and HD 220811. Smoothing was applied to the observed amplitude spectra before plotting and the red stripes mark overtones sequences of $l = 0$ and $l = 1$ modes.

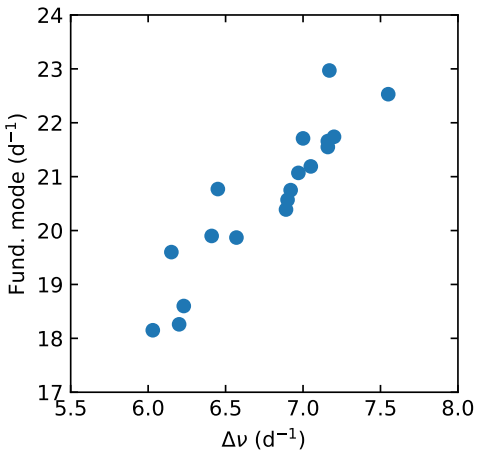

Extended Data Fig. 2 | Correlation between large separation and the frequency of the fundamental radial mode. Symbols show for 18 δ Scuti stars in which the fundamental radial mode is clearly identified. A correlation is expected because both quantities depend on the mean stellar density. We do not expect a perfect correlation due to departures from the asymptotic relation and variations in ϵ from star to star (see Fig. 3c).

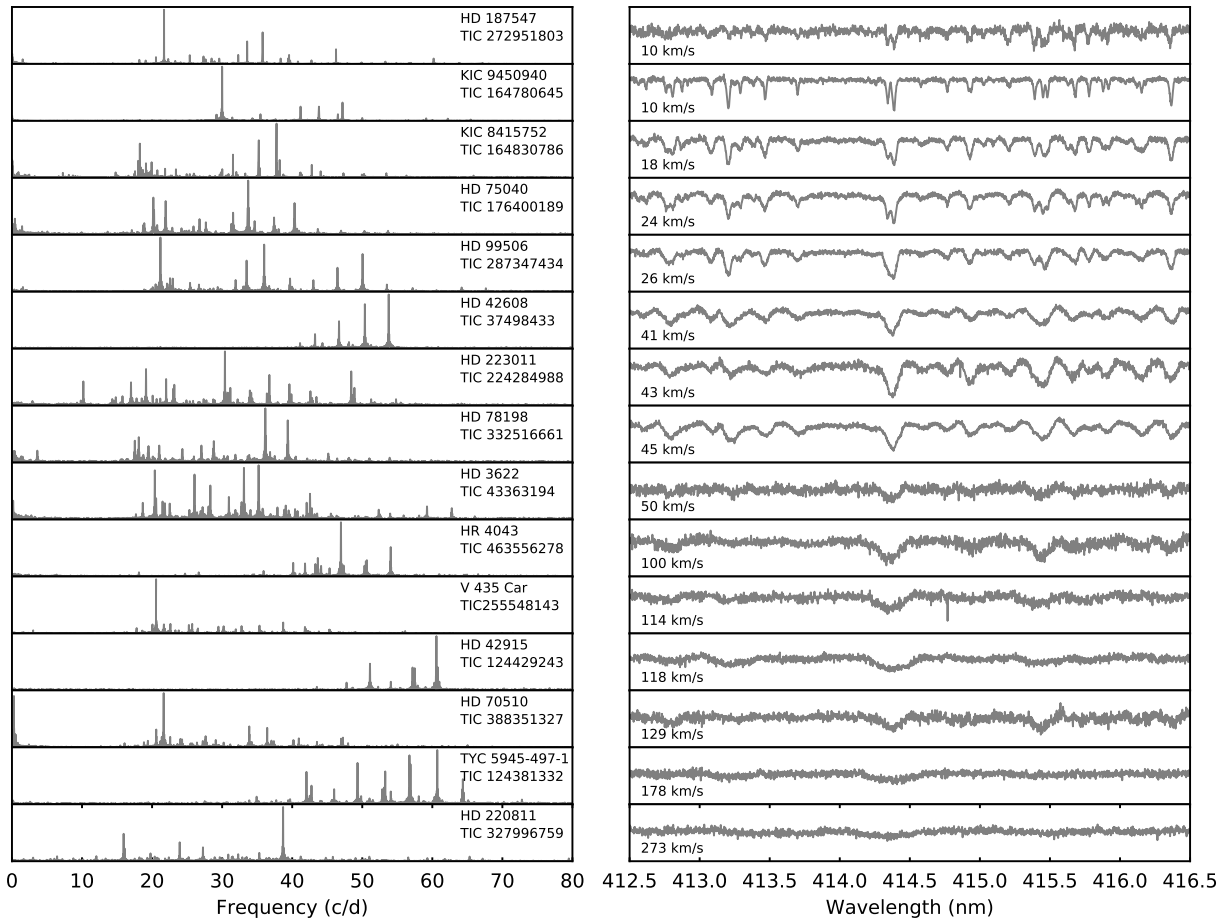

Extended Data Fig. 3 | Fourier amplitude spectra and high-resolution spectra of high-frequency δ Scuti stars. Measured $v \sin i$ values are shown in the right panel and the stars are sorted by increasing $v \sin i$.

Extended Data Table 1 | Properties of high-frequency δ Scuti stars

TIC	HD	Name	V	T_{eff} (K)	L ($L_\odot$)	ρ ($\rho_\odot$)	$\Delta\nu$ (d^{-1})	ϵ	Refs.
281499618	2280		9.13	7510	5.52 ±0.26	0.49±0.06	7.17	1.73	
43363194	3622		7.77	7930	7.86 ±0.35	0.45±0.06	6.89	1.61	
229139161	10779		8.78	7730	8.13 ±0.36	0.39±0.05	6.80	1.63	
231014033	10961		9.39	—	—	—	7.30	1.70	
122615966	17341		9.32	7810	10.05±0.50	0.32±0.05	5.90	1.73	94
122686610	17693		7.80	7880	10.21±0.44	0.33±0.04	6.41	1.61	
274038922	20203		8.85	7970	8.06 ±0.38	0.45±0.05	7.20	1.76	95
159895674	20232		6.88	8060	8.64 ±0.36	0.44±0.05	6.86	1.64	
242944780	24572		9.45	7410	7.25 ±0.36	0.35±0.05	7.20	1.58	95
44645679	24975		7.24	7790	9.20 ±0.39	0.35±0.04	6.23	1.58	
459942890	25248		8.60	—	—	—	7.16	1.55	
9147509	25369		9.68	—	—	—	6.15	1.65	
34197596	25674		8.69	8260	10.20±0.50	0.42±0.05	6.75	1.79	95
71134596	28548		9.22	8510	10.82±0.55	0.45±0.06	7.56	1.67	94, 95
269792989	29783		7.87	—	—	—	6.74	1.79	
589826	30422	EX Eri	6.18	7940	8.42 ±0.35	0.42±0.05	6.52	1.86	96, 97
246902545	31322		9.28	8260	13.19±0.67	0.32±0.04	6.10	1.69	95
259675399	31640		8.06	7690	8.25 ±0.35	0.37±0.05	6.41	1.75	
316920092	31901		9.07	7770	7.74 ±0.39	0.41±0.05	6.97	1.56	27
348792358	32433		9.22	7700	7.32 ±0.35	0.42±0.05	6.95	1.54	
24344701	34282	V1366 Ori	9.92	—	—	—	7.40	1.71	48, 98
31475829	37286	HR 1915	6.26	8080	8.18 ±0.34	0.47±0.06	7.30	—	99
100531058	38597		8.65	8430	10.38±0.47	0.44±0.05	6.90	1.68	95
32763133	38629		8.92	8170	11.27±0.53	0.35±0.04	7.35	1.77	95
270577175	39060	β Pic	3.85	8080	8.49 ±0.39	0.45±0.05	6.95	—	25, 88, 89
282265535	40317		8.45	8700	10.58±0.55	0.51±0.06	6.95	1.63	
408906554	42005		9.54	8030	8.75 ±0.42	0.42±0.05	7.16	1.57	95
37498433	42608		9.85	8170	10.05±0.49	0.40±0.05	7.10	1.57	95
124429243	42915		9.04	8520	12.82±0.68	0.38±0.05	6.40	—	95, 100, 101
150272131	44726		10.38	7890	7.87 ±0.38	0.44±0.05	7.25	1.70	95
34737955	44930		9.42	7320	7.17 ±0.40	0.33±0.05	6.03	1.67	94
255548143	44958	V435 Car	6.74	7660	7.82 ±0.32	0.38±0.05	6.90	1.58	96
117766204	45424		7.18	8060	10.39±0.44	0.36±0.04	6.54	1.86	
172193026	46722		9.29	7810	8.28 ±0.40	0.40±0.05	6.45	1.71	94
148228220	48985		9.04	7710	11.60±0.54	0.25±0.03	7.25	1.56	
78492107	50153		7.03	7820	9.15 ±0.39	0.36±0.05	6.85	1.60	
284348793	54711		9.01	8200	9.22 ±0.45	0.44±0.06	7.08	1.65	
294157254	55863		9.06	7650	7.80 ±0.38	0.38±0.05	6.92	1.57	
278179191	59104		8.50	7360	6.15 ±0.26	0.41±0.05	6.96	1.67	
112484997	59594	V349 Pup	7.32	7800	8.06 ±0.34	0.40±0.05	6.65	1.61	96
306773428	67688		7.66	—	—	—	7.04	1.59	
388351327	70510		6.75	—	—	—	7.16	1.68	
176400189	75040		9.05	—	—	—	6.64	1.58	
332516661	78198		9.50	7340	7.79 ±0.42	0.31±0.04	5.90	1.65	
463556278	89263	HR 4043	6.22	—	—	—	7.02	1.71	

TIC	HD	Name	V	T_{eff} (K)	L ($L_\odot$)	ρ ($\rho_\odot$)	$\Delta\nu$ (d^{-1})	ϵ	Refs.
287347434	99506		8.36	7970	7.58 ±0.37	0.48±0.05	7.05	1.59	[95]
327996759	220811		6.91	—	—	—	6.04	1.82	
316806320	222496		9.48	—	—	—	5.63	1.71	
224284988	223011		6.32	7830	10.49±0.44	0.31±0.04	5.93	1.68	
11199304	290750		9.77	9170	19.14±1.13	0.35±0.05	5.96	—	
11361473	290799	V1790 Ori	10.67	8780	13.21±0.98	0.42±0.06	7.55	1.65	[97, 102]
143381070		SAO 150524	9.46	8030	7.88 ±0.39	0.48±0.06	7.63	—	
349645354		SAO 249859	9.79	7070	7.99 ±0.38	0.23±0.04	5.34	1.69	
431695696		TYC 85-867-1	9.63	7961	8.85 ±0.57	0.40±0.05	7.26	1.61	
124381332		TYC 5945-497-1	9.69	8270	10.02±0.53	0.42±0.05	7.45	1.61	[95]
260161111		TYC 8533-329-1	10.70	8370	9.33 ±0.51	0.48±0.06	7.27	—	[95]
340358522		TYC 8564-537-1	10.59	7490	7.30 ±0.36	0.37±0.05	7.15	1.54	
KIC 7548479	187547		8.40	7470	6.74 ±0.29	0.40±0.05	7.00	1.61	[32, 79]
KIC 8415752		TYC 3132-1272-1	10.67	7780	9.83 ±0.52	0.32±0.05	6.20	1.63	
KIC 9450940			12.68	7920	8.59 ±0.58	0.41±0.06	6.15	1.67	

Stars without parameters (T_{eff}, L and ρ) are close binaries, meaning that those parameters cannot be reliably calculated (see Methods). References indicate classifications as δ Scuti stars [32, 48, 79, 88, 89, 95, 96, 98], λ Bootis stars[94, 97] and members of young moving groups, clusters or stellar streams[25, 27, 99–101, 103].

Extended Data Table 2 | Projected rotational velocities from high-resolution spectroscopy

HD	Name	TIC	v sin i (km s^{-1})	source
2280		281499618	26.4 ± 1.3	AAT+Veloce
3622		43363194	50 ± 6	LCO+NRES
10779		229139161	91 ± 5	AAT+Veloce
10961		231014033	(33 ± 3)	AAT+Veloce
17693		122686610	14 ± 1	AAT+Veloce
20203		274038922	40 ± 25	SALT+RSS
20232		159895674	37 ± 3	AAT+Veloce
24975		44645679	88 ± 4	AAT+Veloce
25674		34197596	160 ± 35	SALT+RSS
28548		71134596	200 ± 50	WHT+ISIS
30422	EX Eri	589826	128	literature[104]
31322		246902545	200 ± 50	SALT+RSS
31640		259675399	136 ± 4	AAT+Veloce
31901		316920092	33 ± 4	LCO+NRES
34282	V1366 Ori	24344701	129 ± 11	literature[87]
37286	HR 1915	31475829	70	literature[105]
38597		100531058	150 ± 40	SALT+RSS
38629		32763133	160 ± 40	SALT+RSS
39060	β Pic	270577175	122	literature[106]
42005		408906554	130 ± 30	SALT+RSS
42608		37498433	41 ± 1	Keck+HIRES
42915		124429243	118 ± 5	Keck+HIRES
44726		150272131	130 ± 40	SALT+RSS
44958	V435 Car	255548143	114 ± 11	LCO+NRES
48985		148228220	40 ± 4	AAT+Veloce
54711		284348793	50 ± 2	AAT+Veloce
55863		294157254	99 ± 5	AAT+Veloce
70510		388351327	(94 ± 10)	LCO+NRES
75040		176400189	(24 ± 3)	Keck+HIRES
78198		332516661	45 ± 1	Keck+HIRES
89263	HR 4043	463556278	(100 ± 7)	Keck+HIRES
99506		287347434	26 ± 2	Keck+HIRES
220811		327996759	(261 ± 40)	Keck+HIRES & LCO+NRES
223011		224284988	43 ± 2	LCO+NRES
	TYC 5945-497-1	124381332	178 ± 37	Keck+HIRES
	TYC 8533-329-1	260161111	100 ± 30	SALT+RSS
187547		KIC 7548479	10 ± 2	literature[79]
	TYC 3132-1272-1	KIC 8415752	18 ± 1	Keck+HIRES
		KIC 9450940	10 ± 1	Keck+HIRES

Values of v sin i in parentheses indicate a close binary (see Methods), meaning the measurement may not be reliable.